JNeurosci
THE JOURNAL OF NEUROSCIENCE

Research Articles: Cellular/Molecular

A Novel and Functionally Diverse Class of Acetylcholine-gated Ion Channels

https://doi.org/10.1523/JNEUROSCI.1516-22.2022

Cite as: J. Neurosci 2023; 10.1523/JNEUROSCI.1516-22.2022

Received: 8 August 2022
Revised: 2 December 2022
Accepted: 14 December 2022

A Novel and Functionally Diverse Class of Acetylcholine-gated Ion Channels

Abbreviated title: Novel Acetylcholine-gated Ion Channels

Iris Hardege *[1], Julia Morud *[1], Amy Courtney[1], William R Schafer [1,2]

Affiliations

[1] MRC Laboratory of Molecular Biology, Francis Crick Avenue, Cambridge, CB2 0QH, United Kingdom

[2] Department of Biology, KU Leuven, 3000, Leuven, Belgium

* These authors contributed equally to this work

Corresponding Author: William R Schafer, wschafer@mrc-lmb.cam.ac.uk

Conflict of interest statement

The authors declare no competing interests.

Abstract

Fast cholinergic neurotransmission is mediated by acetylcholine-gated ion channels; in particular, excitatory nicotinic acetylcholine receptors play well established roles in virtually all nervous systems. Acetylcholine-gated inhibitory channels have also been identified in some invertebrate phyla, yet their roles in the nervous system are less well understood. We report the existence of multiple new inhibitory ion channels with diverse ligand activation properties in *C. elegans*. We identify three channels, LGC-40, LGC-57 and LGC-58, whose primary ligand is choline rather than acetylcholine, as well as the first evidence of a truly polymodal channel, LGC-39, which is activated by both cholinergic and aminergic ligands. Using our new ligand-receptor pairs we uncover the surprising extent to which single neurons in the hermaphrodite nervous system express both excitatory and inhibitory channels, not only for acetylcholine but also the other major neurotransmitters. The results presented in this study offer a new insight into the potential evolutionary benefit of a vast and diverse repertoire of ligand-gated ion channels to generate complexity in an anatomically compact nervous system.

Significance statement

Here we describe the diversity of cholinergic signalling in the nematode *C. elegans*. We identify and characterise a novel family of ligand-gated ion channels and showed that they are preferentially gated by choline rather than acetylcholine and expressed broadly in the nervous system. Interestingly, we also identify one channel gated by chemically diverse ligands including acetylcholine and aminergic ligands. By using our new knowledge of these ligand-gated ion channels we built a model to predict the synaptic polarity in the *C. elegans* connectome. This model can be used for generating hypotheses on neural circuit function.

Introduction

Rapid signalling through neuronal networks is essential for producing coordinated behaviours in animals. At the fundamental level, fast neuronal transmission is mediated through neurotransmitter release resulting in activation of ion channels on the postsynaptic neuron. In the textbook view, based predominately on mammalian systems, there are two major excitatory neurotransmitters, glutamate, and acetylcholine (ACh), and two inhibitory neurotransmitters, GABA (*gamma aminobutyric acid*) and glycine, which both switch from excitatory to inhibitory signalling during development in mammalian nervous systems (Kirsch, 2006; Tyzio et al., 2007). Glutamate acts through a family of tetrameric ligand-gated cation channels, while the remaining neurotransmitters activate the pentameric ligand-gated ion channel (LGICs) superfamily.

Although LGICs are highly conserved across phyla, ligand binding properties and ion selectivity diverge significantly, resulting in a large diversity of mechanisms by which small molecules acting via LGICs can influence the activity in neuronal circuits particularly when channels from invertebrate phyla are considered. For example, insects and nematodes express inhibitory glutamate receptors from the pentameric ligand-gated ion channel superfamily, localised both in neurons and muscles, which are the main targets for achieving the anthelminthic effect of the drug ivermectin (Cully et al., 1994, 1996). Many animals including insects, nematodes and mammals also express LGICs which can be gated by aminergic ligands, including histamine-gated chloride channels (Gisselmann et al., 2002), important for fly visual processing, a number of nematode channels, involved in learning and motor control (Pirri et al., 2009; Morud et al., 2021), as well as the excitatory mammalian 5-HT_3 receptor (Kondo et al., 2014; Lombaert et al., 2018). Even more divergent roles for LGICs have been identified in marine species, where LGICs gated by terpenes and chloroquine function as chemoreceptors in octopus (van Giesen et al., 2020).

Pentameric ligand-gated ion channels can be subdivided into two large clades, the first containing the nicotinic receptors and their paralogues including the serotonin 5-HT_3 receptors, and the other containing channels more closely related to $GABA_A$ receptors (Jones and Sattelle, 2008). The *C. elegans* genome contains several subfamilies which appear to have diversified independently from vertebrate channels during evolution, leading to the existence of several nematode specific LGIC subfamilies. The *C. elegans* genome contains a number of $GABA_A$-like subfamilies, including genes encoding both anion and cation-selective channels (Ranganathan et al., 2000; Yassin et al., 2001; Putrenko et al., 2005; Ringstad et al., 2009; Margie et al., 2013; Jobson et al., 2015). One of these subfamilies consist of genes for both anion and cation selective monoamine-gated channels, another of acetylcholine-gated anion channels or channels that are still largely uncharacterised. One member in one of these subgroups, LGC-40 (ligand-gated channel-40), has previously been reported to be a low affinity serotonin-gated channel also gated by acetylcholine and choline (Ringstad et al., 2009). The properties of the remaining channels in these subgroups, including their ligands, ion selectivity, and expression patterns, are currently unknown.

Here we describe the ligand activation profiles and pharmacological characteristics of five new *C. elegans* LGICs which are all activated by the cholinergic ligands acetylcholine and/or choline. One of these, LGC-39, forms a homomeric anion channel which in addition to being activated by acetylcholine, appears to be polymodal and is also activated by monoamines. Using publicly available single cell RNAseq expression data (Taylor et al., 2021) together with our new electrophysiological data, we predict the polarity of synapses in the worm connectome, as well as intracellular localisation patterns for uncharacterised LGICs. These results highlight the unexpected functional diversity of cholinergic signalling in the *C. elegans* nervous system.

Materials and Methods

C. elegans culture

Unless otherwise specified, *C. elegans* hermaphrodite worms were cultured on NGM agar plates with OP50 (Stiernagle, 2006). A full list of strains used in this study can be found in table 4-1.

Xenopus laevis oocytes

Defolliculated *Xenopus laevis* oocytes were obtained from EcoCyte Bioscience (Dortmund, Germany) and maintained in ND96 (in mM: 96 NaCl, 1 $MgCl_2$, 5 HEPES, 1.8 $CaCl_2$, 2 KCl) solution at 16° C for 3-7 days.

Molecular biology

Unless otherwise specified, cDNA sequences of *C. elegans* genes were cloned from wildtype N2 worm cDNA (generated by reverse transcription PCR from total worm RNA using Q5 polymerase (New England Biosciences)). Where multiple isoforms are present isoform a was used. LGC-39 cDNA was generated by gene synthesis (ThermoFischer). For expression in *Xenopus* oocytes, ion channel cDNA sequences were cloned into the KSM vector downstream of a T3 promoter and between *Xenopus* β-globin 5' and 3'UTR regions using the HiFi assembly protocol (New England Biosciences). *C. elegans* expression constructs were also generated using the HiFi assembly protocol (New England Biosciences) into the pDESTR4R3II backbone. *C. elegans* gDNA sequences were cloned from wildtype N2 gDNA and expression verified by the addition of GFP or mKate2 introduced on the same plasmid after an intercistronic splice site (SL2 site). Unless otherwise specified promoter sequences consist of approximately 2kb of gDNA upstream of the start codon. A full list of primers used in this study can be found in table 4-2.

CRISPR/Cas9-mediated gene manipulation

Endogenous tagging of the M3/4 cytosolic loop of *C. elegans* LGIC proteins with GFP was carried out either using the SapTrap protocol (Schwartz and Jorgensen, 2016; Dickinson et al., 2018) for *lgc-39(lj121)*, or by SunyBiotech (Fuzhou, China) for *lgc-57(syb3536)*, *lgc-58(syb3562)*, and *lgc-40(syb3594)*.

RNA synthesis and microinjection

CRNA was synthesised *in vitro* using the T3 mMessage mMachine transcription kit according to manufacturer's protocol to include a 5' cap (Thermo Fischer Scientific). Prior to injection RNA was purified using the GeneJET RNA purification kit (Thermo Fischer Scientific). Size sorted and defolliculated *Xenopus* oocytes (Ecocyte) were placed individually into 96-well plates and injected with 50 nL of 500 ng/µL RNA using the Roboinject system (Multi Channel Systems GmbH). When two constructs were co-injected the total RNA concentration remained 500 ng/µL, with a 1:1 ratio of the components. Injected oocytes were incubated at 16°C in ND96 until the day of recording, typically between 3-6 days post injection.

Two-Electrode Voltage Clamp (TEVC) recording and data analysis

TEVC recordings were carried out using either the Robocyte2 system or a manual set up with an OC-725D amplifier (Multi Channel Systems GmbH). Glass electrodes with a resistance ranging from 0.7-2 MΩ were pulled on a P1000 Micropipette Puller (Sutter). Electrodes contained AgCl wires and backfilled with a 1.5 M KCl and 1 M acetic mixture. Unless otherwise stated, oocytes were clamped at -60mV. Continuous recordings at 500Hz were taken during application of a panel of agonists (ACh, choline, dopamine, tyramine, GABA,

glutamate, histamine, 5-HT, betaine and octopamine), each agonist was washed on for 10 s, unless specified otherwise, followed by a 10-30 s wash (depending on effect size of the first agonist), data was gathered over at least two occasions, using different batches of oocytes. Typical perfusion rate was 60 µl/s with a bath volume of approximately 80 µl, predicting full solution exchange within 1.5-2 s. However, the timing of currents in our traces indicate that the true exchange rate varies. Solution mixing is likely affected by variations in cell and electrode position in each well, which is not controlled or monitored in our automated system. Data was recorded using the RoboCyte2 control software, or with WinWCP for manual recordings, and filtered at 10 Hz. Dose response protocols used 10 s (unless specified otherwise) agonist application pulses with 60 s of wash in ND96 between each dose. Doses for each dose response curve were adjusted to ensure that both a lower and upper plateau in current were reached. Where this was not possible due to solubility or oocyte health, the highest dose possible was used. Data was gathered over at least two occasions, using different batches of oocytes. Ion selectivity was detected using a voltage ramp protocol from -80mV to +60mV (20mV/s) in the presence of the primary agonist in three different solutions: ND96, NMDG (Na^+ free) and Na Gluconate (low Cl^-) solutions.

Confocal and cell ID

Worms were prepared and immobilised with 75 mM NaAzide in M9 and mounted onto 2% agarose in M9 pads. Image stacks were acquired with a 63x water immersion lens on a Leica SP8 or STED or using a 40x oil immersion objective on a Zeiss LSM780. Collapsed z-stack images were generated in Fiji/Image J. Neurons expressing fluorescent reporters were identified by cell shape, position and crossing with the multicolour reference worm NeuroPAL (Yemini et al., 2020).

Synaptic polarity prediction

Inhibitory and excitatory chemical synapse prediction for ACh, Glu and GABA synapses were based upon expression levels of appropriate LGICs in postsynaptic cells. Chemical and electrical connectome data was obtained from Wormweb (http://wormweb.org/details.html), LGIC expression data was taken from the Cengen project using threshold level 4 (Taylor et al., 2021), ligand and ion selectivity for each channel was based upon this work. Previous work and predictions are presented in Table 1. Binary expression of LGICs for each neurotransmitter in each neural class were based upon expression and characterised in four groups: only excitatory, only inhibitory, both excitatory and inhibitory or none. These binary values were used to make the binary expression heatmap. Overall polarity of a synapse was calculated by summing the expression of all inhibitory and all excitatory LGICs for a given neurotransmitter in each cell class. The sum inhibitory was then taken from the sum of excitatory expression, resulting in an overall positive or negative signed expression in each neural class for each neurotransmitter. The ratio of these sums was also calculated to indicate the strength of polarity. It was assumed that each LGIC in each neural class is present equally at all synapses, therefore each incoming connection could be assigned a polarity based upon its receptor expression for that neurotransmitter. The resulting network with polarity was imported into cystoscope (Shannon et al., 2003) for plotting and further analysis. Analysis scripts can be found on GitHub at hiris25/Worm-Connectome-Polarity.

Expression and cholinergic synapse analysis

The total number of cholinergic input or output synapses was calculated for each neural class by summing the number of presynapses for each cell that received a synapse from an ACh-producing neuron (incoming synapses), or the total number of post-synapses an ACh-producing neural class makes (outgoing synapses). ACh-producing cells were described by

(Pereira et al., 2015), the assumption was that all synapses made by an ACh-producing cell also release ACh, even when this cell co-transmits another neurotransmitter. Synapse number for each neuron was taken from (White, 1986). Expression data was obtained from (Taylor et al., 2021) using a threshold of 2. Neural classes were sorted by ACh in or out degree and the expression of each gene was mapped using a heatmap with an upper threshold of 500. For correlation plots, cells that did not express a receptor, were removed from the analysis. Correlation between expression level and ACh in, or out, degree was mapped using relplot in python's seaborn package, confidence intervals were placed at 68%, corresponding to the standard error of the estimate.

Experimental design and statistical analysis

For TEVC dose response data, peak current for each dose was normalised to the oocyte maximum current using a custom-built python script (Morud et al., 2021), unless otherwise stated this was done using I/Imax, where Imax is the largest current generated by the individual oocyte, irrelevant of which dose this occurred in. Since responses can vary between oocytes Imax may occur at a particular dose in some oocytes injected with a given channel gene and at a different dose in others, leading to an averaged normalised response that peaks at less than 1. Normalised data was imported into Graphpad (Prism) and fitted to either a three or four parameter nonlinear Hill equation (as stated in figure legends) to obtain the highest degree of fit and calculate the EC_{50}. Antagonist dose responses and ion selectivity recordings were carried out using the EC_{50} concentration of the primary agonist. Antagonist dose response protocols used 10 s agonist + antagonist windows, with 60 s of ND96 washes between doses. The agonist concentrations remained constant. Antagonist IC_{50} values were calculated using a second custom-built python script (Morud et al., 2021). Normalised data was imported into Graphpad (Prism) and fitted to a three-parameter nonlinear Hill equation to

calculate the IC_{50}. TEVC ion selectivity data was normalised to max current and ΔE_{Rev} was calculated using a custom-built python script (Morud et al., 2021). The resulting individual values or mean, SEM and n for each construct was imported into GraphPad for further plotting and statistical analysis. Statistically significant differences in ΔE_{Rev} were calculated in GraphPad using a two-way ANOVA with Tukey's correction for multiple comparisons. A representative normalised trace for each construct was also generated in Graphpad. N numbers are stated in respective figure legends.

Data and code availability

Python scripts can be found at on GitHub at hiris25/TEVC-analysis-scripts and hiris25/Worm-Connectome-Polarity. Aggregated data used for analysing TEVC data are available upon request from the Lead Contact. Further information and requests for *C. elegans* strains and plasmids is to be sent to and will be fulfilled by the Lead Contact William R Schafer, wschafer@mrc-lmb.cam.ac.uk

Results

Deorphanisation of Uncharacterised LGICs Reveals Diversity of Cholinergic Channels

The *C. elegans* genome encodes a diverse superfamily of pentameric ligand-gated ion channels (LGICs), of which several subfamilies are poorly characterised. Here we investigate the diverse group (for details of group naming see: Jones et al., 2007; Jones and Sattelle, 2008; Hobert, 2013), which consists of 3 subgroups named after a channel from each group; the LGC-45 group, the LGC-41 group, and the GGR-1 group (here renamed to LGC-57 group) (Figure 1A) and contains many channels whose activating ligand and function are unknown, known as orphan channels. To deorphanise and investigate the properties of these

channels, we first expressed each channel gene in *Xenopus* oocytes and tested for current activation during the perfusion of a panel of neurotransmitters. Despite their homology to vertebrate $GABA_A$ and glycine receptors (the source of the name GGR-1), we observed no activation of any members of the LGC-57 group (or any diverse group channels) by either GABA or glycine. Instead, we found three closely related channels of the LGC-57 group: LGC-57 (formerly GGR-1), LGC-58 (formerly GGR-2) and LGC-40 to be specifically gated by choline and acetylcholine (Figure 1B, Figure 1-2A). All three channels showed a preference for choline, with EC_{50} values 2.5 to 3-fold lower for choline than acetylcholine (Figure 1C, Figure 1-5). These findings parallel a previous report that LGC-40 forms a choline and acetylcholine-gated channel, although in contrast to that report we did not observe serotonin responses (Ringstad et al., 2009). We did not observe currents in response to any of the tested compounds for the remaining members of the diverse group (LGC-42, LGC-44, LGC-45 or co-expressed as LGC-44/LGC-45), as well as LGC-32, LGC-33, and LGC-34, which although did not fall within this group in our phylogenetic analysis (Figure 1-1), have previously been described as part of the diverse group (Hobert, 2013) (Figure 1-2B-C, Table 1-1). The lack of agonist-induced currents may be because the channel was poorly expressed, the correct ligand was not tested or because they function only as components of heteromeric complexes. The remaining member of the LGC-57 group, LGC-39 showed unusual activation properties which will be discussed below.

In addition to the diverse group channels, many other *C. elegans* LGICs lack identified ligands. For example, while several members of the ACC group (Acetylcholine-gated Chloride Channels) of LGICs have been shown to form acetylcholine-gated chloride channels, four members of this subfamily *(acc-4, lgc-47, lgc-48,* and *lgc-49)* had not previously been characterised (Figure 1A, in red). Upon expression in *Xenopus* oocytes, we found that one of these channels, LGC-49, formed a homomeric acetylcholine-gated channel

with an EC_{50} of 19 μM (Figure 1C, Figure 1-2D, Figure 1-5), similar to the EC_{50} values published for other members of this group (Putrenko et al., 2005; Takayanagi-Kiya et al., 2016). Unlike the members of the LGC-57 group, which showed activation by both acetylcholine and choline, LGC-49 showed no significant activation by choline. This channel further differed from the members in the diverse group by its inability for fast reactivation, which restricted data normalisation as per I/I_{max} (Figure 1C). It should also be noted that the EC_{50} values produced in *Xenopus* oocytes do not necessarily mimic the endogenous in vivo EC_{50} of these channels.

None of the ligands tested here induced currents for ACC-4, LGC-47, or LGC-48 when expressed alone (Figure 1-2E-F, Table 1-1). We note though that a previous study provided evidence that ACC-4 acts as part of a heteromeric complex with ACC-2 (Putrenko et al., 2005). We therefore chose to test two combinations of channels from the ACC group: LGC-47 with ACC-1 and LGC-48 with ACC-4, we did not note any ligand induced activity for LGC-48/ACC-4 (Figure 1-2E). However, we did observe a 10-fold right shift in the acetylcholine EC_{50} between oocytes expressing ACC-1 alone and ACC-1/LGC-47 co-expressing oocytes, with the ACC-1/LGC-47 combination showing a higher EC_{50} (Figure 1-2G). This data suggests that ACC-1 and LGC-47 may form a heteromeric channel, however, further detailed characterisation of this combination will be required to validate the existents of a functional heteromer. Given the vast number of possible heteromeric combinations within the ACC group it may be that these orphan channels are part of more complex channel compositions not tested here. Finally, we attempted to improve expression of the remaining orphan LGICs from the diverse and ACC groups: LGC-42, LGC-44, LGC-45, LGC-47, and LGC-48, by co-expressing these channels with RIC-3, which has previously been shown to enhance expression of nematode nAChRs in *Xenopus* oocytes (Halevi et al., 2002) (Figure 1-6). However, we did not observe any agonist induced currents in oocytes co-expressing these

channels and RIC-3, that were greater than those observed in oocytes expressing RIC-3 alone (Figure 1-6B).

We next investigated the ion selectivity of the newly deorphanised channels by carrying out ion substitution experiments in oocytes expressing LGC-40, LGC-57, LGC-58, or LGC-49. For all these channels we observed significant reversal potential shifts following substitution of standard high chloride (NaCl) buffer for low chloride (Na Gluconate), but not following substitution with sodium-free (NMDG) solution, indicating selectivity for anions over cations for all the tested channels (Figure 2A-B). We also tested the previously deorphanised channel LGC-46 (Takayanagi-Kiya et al., 2016; Liu et al., 2017) which to date lacked ion selectivity data. This channel likewise showed reversal shifts characteristic of an anion selective channel (Figure 2A-B). Interestingly, all members of the LGC-57 group possess a PAR motif (Proline-Alanine-Arginine), located in the M1-2 intracellular loop (Figure 1-3A), which has been shown to impart anion selectivity to LGICs (Wotring et al., 2003). Although several uncharacterised members of the ACC group have sequences that diverge from the PAR motif, both LGC-49 and LGC-46 contain the PAR motif sequence (Figure 1-3A). Thus, the PAR motif appears to correlate with anion selectivity in both the LGC-57 and ACC groups of nematode acetylcholine-gated LGICs.

Cholinergic Channels Display Diverse Antagonist Binding Properties

To understand if there are further functional differences between the channels deorphanised in this study, we exposed each channel to three cholinergic antagonists, mecamylamine, strychnine and d-tubocurarine. Strychnine and d-tubocurarine have been shown to compete with the full agonist for the ligand binding domain, although their binding mechanisms vary between LGICs of different classes (Brams et al., 2011); in contrast, mecamylamine has been shown to interact with the transmembrane regions of mammalian

nAChRs (Bondarenko et al., 2014). Indeed, we saw that the antagonistic profile differed significantly between the newly deorphanised channels. For example, within the LGC-57 group the two smallest antagonists, mecamylamine and strychnine, had similar IC_{50} values for LGC-40, LGC-57 and LGC-58 (Figure 2C, Figure 2-1). However, tubocurarine, the largest molecule of the antagonists, displayed an 11-fold shift in IC_{50} for LGC-57 compared to LGC-58 and LGC-40 (Figure 2C, Figure 2-1). Thus, the binding capabilities of tubocurarine on LGC-57 differs substantially from that of its closest family members LGC-58 and LGC-40. Likewise, in the ACC group, LGC-46 and LGC-49 could both be blocked by mecamylamine, strychnine and tubocurarine (Figure 2C, Figure 2-1). These dissimilarities again highlight the discrete differences between channels from the same subfamily, which may have similar ligand-activation profiles for endogenous ligands. Interestingly, tubocurarine was the most potent blocker for the ACC group channels LGC-46 and LGC-49, whereas this antagonist was the least effective of the channels tested in the LGC-57 group.

We also tested the channels' responses to repeated stimulation by their primary ligand. We found LGC-40 to be sensitive to repeated stimulation, displaying a significant difference in ratio between the first and second pulse after 10, 30 and 60 s of washing intervals (Figure 2D-E). In contrast, all other channels were capable of fast activation intervals as they did not display any decrease in peak amplitude after repeated stimulation (Figure 2D-G). Thus, the mechanism of LGC-40 activation appears to be different to the remainder of the group. However, due to the naturally slow kinetics in *Xenopus* oocytes, it is hard to draw any conclusion with regards to desensitisation or receptor wear down based on these results.

LGC-39 is a Novel Polymodal Channel Activated by Cholinergic and Aminergic Ligands

One channel from the LGC-57 group, LGC-39, showed distinct ligand activation properties from the rest of the group. Unlike the other LGC-57 subfamily members, LGC-39 showed relatively little activation by choline (Figure 3A, Figure 1-2H). Moreover, while acetylcholine activated LGC-39 strongly (with an EC_{50} of 1290μM), the most potent ligands for LGC-39 were the monoamines octopamine and tyramine (with EC_{50} values of 921 μM and 686 μM respectively; Figure 3A-B, Figure 1-5). Although EC_{50} values for LGC-39 were higher than those we observed for other members of the diverse group, EC_{50} values in this range are seen for related channels such as the mammalian $GABA_A$ receptors when expressed in *Xenopus* oocytes (Karim et al., 2013). In addition, LGC-39 also displayed small currents in response to dopamine (Figure 3A, Figure 1-2H). Both activation by aminergic or cholinergic ligands resulted in Hill slope values above 1, suggesting each ligand binds in a positive cooperative manner on the channel (Cattoni et al., 2015). Like other members of the LGC-57 family, LGC-39 contains the PAR sequence (Figure 1-3A), and LGC-39-expressing oocytes showed reversal potential shifts in response to chloride but not sodium substitution (Figure 3C). Thus, *lgc-39* appears to encode a homomeric anionic and polymodal channel, capable of being activated by both aminergic and cholinergic neurotransmitters (Figure 3A-C).

We tested the effects of cholinergic and non-cholinergic antagonists on LGC-39 currents evoked by different activating ligands. In the presence of acetylcholine, LGC-39 could be blocked by the cholinergic antagonists mecamylamine, strychnine and tubocurarine (Figure 3D). In contrast, the octopamine response could not be blocked by mecamylamine or strychnine. Surprisingly, strychnine, without the presence of an activating ligand, acted as a partial agonist, since it induced a small current with an EC_{50} of 7.5 μM (Figure 3E). The non-cholinergic blockers, epinastine, a selective octopaminergic blocker (Packham et al., 2010) and yohimbine, an α2 adrenergic blocker, both blocked acetylcholine induced currents with IC_{50} values of 1 μM and 4 μM respectively (Figure 3D), however only yohimbine blocked

367 octopamine induced currents with an IC_{50} of 28 μM. Interestingly, epinastine also acted as an
368 agonist both in the presence and absence of octopamine with an EC_{50} of 10 μM (Figure 3E).
369 To further separate the functionality of the ligands, we also investigated if repeated activation
370 by the different ligands influenced the ability for reactivation of LGC-39 differently (Figure
371 3F). No difference was seen for any wash interval between the ligands, which could suggest
372 that all ligands occupy the binding site in a similar time frame or that the recovery time for
373 the channel is independent of the activating ligand.
374
375 **Cholinergic Channels show Broad and Varied Expression in The *C. elegans* Nervous**
376 **System**
377 To gain insight into the roles of cholinergic LGICs in the nervous system, we
378 generated reporter lines to characterise their neural expression patterns. We used a similar set
379 of fluorescent reporter lines to characterise the expression pattern of the newly deorphanised
380 LGICs, by using transcriptional reporter transgenes in which the upstream promoter of the
381 *lgc* gene drives the expression of a fluorescent protein. We then identified transgene-
382 expression based upon location, morphology and known marker lines. Using such a
383 transcriptional reporter, we observed primarily neuronal expression of the genes in the LGC-
384 57 group, with little overlap observed in the neurons that were expressing reporters for *lgc-*
385 *40*, *lgc-57,* and *lgc-58* (Figure 4A-C). *lgc-40* was expressed in many pharyngeal neurons
386 (M2, M3, MC, MI, I2), *lgc-57* in the A-class and B-class motorneurons of the ventral cord,
387 and *lgc-58* in the egg-laying motorneurons (VCs; *lgc-57* was also observed in a subset of
388 VCs). This suggests that these channels are likely to exist primarily as homomers *in vivo* and
389 function in distinct target neurons. Further we observed the reporter for *lgc-39* in a range of
390 interneurons and motor neurons, including the AVA premotor interneurons (Figure 4E). In
391 addition to receiving extensive cholinergic input, the AVA neurons are the major synaptic

target for the only octopaminergic neurons, the RICs, suggesting that LGC-39 may be exposed to both octopamine and ACh *in vivo* (Figure 4F) and may be involved in both cholinergic and octopaminergic synaptic transmission. Finally, we found that the ACC group channel, *lgc-49,* was expressed in sensory neurons, including posterior sensory neurons such as ALN and PLN (Figure 4D).

We also used reporters to analyse the expression pattern of several still-orphan LGICs, from the diverse and ACC groups, including *lgc-42, lgc-47, lgc-48, lgc-43* and *lgc-45*, as well as the previously deorphanised ACh-gated channel *lgc-46* (Takayanagi-Kiya et al., 2016) (Figure 4-1A-D). These reporters also showed diverse and distinct patterns of expression, primarily in neurons. For example, *lgc-46* was broadly expressed in several neurons, mostly in the head (Figure 4-1D). Most of the orphan channels were also expressed specifically in neurons; for *lgc-47* this expression was unusually broad, encompassing sensory, motor, and interneurons (Figure 4-1A). Interestingly, we noted that the expression of *lgc-47* overlaps with the reported single cell RNAseq expression profile of *acc-1* in several classes of motor neurons (Taylor et al., 2021), such as the SMDs, RMDs, M3, and DA neurons (Table 4-3). This, in combination with the functional data from co-expressing these in *Xenopus* oocytes (Figure 2-1F-G), may suggest that LGC-47 and ACC-1 are able to form a heteromeric channel. In contrast, *lgc-48* was expressed only in a single pair of neurons, the ADL chemosensory neurons (Figure 4-1B). Interestingly, the two orphan channels, *lgc-43,* and *lgc-45,* which both lack a PAR sequence and may thus encode cationic channels (Figure 1-3A), did not appear to be expressed in any neuronal tissue, but instead in the hypodermis (Figure 4-1B). Our reporter expression patterns also aligned well with single cell RNAseq data from the CeNGEN project (Taylor et al., 2021) (Table 4-3). Together, these data suggest that these channels play various roles in, and outside, the nervous system.

Excitatory and Inhibitory Ionotropic Acetylcholine Receptors are Co-expressed in Many Neurons

Our fluorescent reporter expression analysis indicated that many of the newly deorphanised inhibitory acetylcholine-gated channels in this study are expressed in neurons previously shown to also express excitatory acetylcholine-gated channels (Raizen et al., 1995; Barbagallo et al., 2010). These results imply that acetylcholine, as an inhibitory neurotransmitter, may have a larger role than previously appreciated, and that acetylcholine contributes to both inhibitory and excitatory events in many neurons. To determine the extent to which excitatory and inhibitory ionotropic receptors, for the same neurotransmitter, are expressed in individual neural classes, we made use of the single cell RNAseq dataset from *C. elegans* neurons (Taylor et al., 2021). We first generated a complete list of ionotropic receptors for each of the three classical neurotransmitters acetylcholine, GABA and glutamate (Table 5-1). Since channels with unknown ligand-identity would have the potential to bias predictions, we predicted the ligand and ion selectivity of orphan channels based upon homology with closely related characterised channels, and the presence, or absence, of a PAR motif in the M1-2 intracellular loop (see Methods).

From this analysis, we found a remarkable frequency of neural classes that co-express both inhibitory and excitatory ionotropic receptors for the same neurotransmitter. This was particularly notable for acetylcholine, for which over 60% of the neural classes expressed both excitatory and inhibitory acetylcholine-gated channels. In contrast, GABA-gated channels were more biased toward inhibition, with only 9% of neural classes expressing both types of receptors and over 40% of neural classes expressing only inhibitory GABA-gated channels (Figure 5A, Figure 5-1). To make generalised predictions of synaptic polarity, we summed expression of inhibitory and excitatory ionotropic receptors, for each neurotransmitter, in each neural class and assigned synapse polarity based on the most

prevalent receptors in each neural class, assuming that all receptors in a cell are present equally at all synapses (Figure 5C, Figure 5-2). This approach does not take heteromerisation of different subunits, nor differences in synaptic strength into account and should therefore be considered a generalised prediction. The analysis suggested that the majority of acetylcholine and glutamate synapses are excitatory, and most GABAergic synapses are inhibitory, though this varied significantly for individual connections (Figure 5B).

To examine the validity of our polarity predictions we investigated the sign prediction using previously characterised neuronal circuits. We picked the well-studied locomotion circuit (Chalfie et al., 1985) consisting of the interneurons AVD, AVE and AVA, which initiate reversals, and PVC and AVB that initiate forward movement. Most of our predicted connection polarities (Figure 5D) were consistent with circuit data from previous studies, such as the excitatory connection between AVA and the VA and DA motor neurons, which is involved in controlling reverse locomotion, as well as the excitatory connection from the sensory neuron ASH to the reverse command neuron AVA (Mellem et al., 2002; Piggott et al., 2011). We also observed connections which appeared counter intuitive such as an inhibitory acetylcholine connection from AVD to AVA, two interneuron pairs thought to be co-ordinately active during reverse locomotion (Faumont et al., 2012) (Figure 5D). While some studies have proposed additional inhibitory connections within this circuit (Rakowski and Karbowski, 2017), AVA neurons express several acetylcholine-gated channels and has a relatively low ratio of inhibitory to excitatory ionotropic receptor expression (1:3), upon which this prediction was made. This suggests that some connections may indeed be both inhibitory and excitatory, especially where a neuron expresses a large range of different channels and receives input from many different neural classes. Connections such as these require further *in vivo* investigations to address these predictions.

Determining Synaptic Localisation of LGICs

We reasoned that the single cell RNAseq dataset (Taylor et al., 2021) might also be useful for predicting the intracellular localisation of cholinergic LGICs, as presynaptic ionotropic receptors would be predicted to be expressed in cholinergic neurons, while postsynaptic ionotropic receptors should be expressed in neurons receiving cholinergic input. To assess the correlation between the number of acetylcholine synapses a neuron makes ('outgoing ACh synapses') or receives ('incoming ACh synapses'), with the expression level of cholinergic LGICs, we produced two heatmaps showing the expression of acetylcholine-gated channels, with neural classes ranked by the total number of incoming or outgoing acetylcholine synapses (Figure 6A-B). This analysis highlights that the expression of some ACC group channels, in particular, *lgc-46,* correlate with both the number of incoming and outgoing ACh synapses (Figure 6C-D, Figure 6-1), which is in line with previous studies describing both a pre- and post-synaptic role for LGC-46 (Takayanagi-Kiya et al., 2016; Liu et al., 2017). This correlation suggests that these channels may be acting either pre- or post-synaptically. In contrast, members of the choline and acetylcholine-gated LGC-57 group, *lgc-40, lgc-57,* and *lgc-58*, showed little correlation with either incoming or outgoing synapses (Figure 6C-D). Surprisingly for this subgroup, several cells with high acetylcholine connectivity showed low channel expression level (Figure 6C-D). This may be suggestive of an extrasynaptic role for these channels, however further evidence is required to make these assumptions.

To empirically assess the synaptic localisation of cholinergic LGICs, we generated endogenous GFP-tagged CRISPR lines for members of the LGC-57 subgroup, including *lgc-39*, *lgc-40, lgc-57,* and *lgc-58* and (Figure 7A-D). In all cases GFP was inserted in the intracellular M3/4 loop and the function of the resulting chimeric protein was verified in *Xenopus* oocytes (Figure 7-1A). We observed a clear difference in the localisation pattern for

these channels. LGC-39::GFP was localised in distinct punctate structures both in the nerve ring and along the ventral cord, suggestive of synaptic localisation (Figure 7A), and consistent with the positive correlation between *lgc-39* expression and incoming and outgoing acetylcholine synapses (Figure 6A-D). Members of the choline-gated LGC-57 group however showed diffuse protein expression. LGC-40::GFP appeared to have diffuse expression in the nerve ring, and touch receptor neurons, with cell bodies often being visible (Figure 7B). Notably, cell body LGC-40::GFP expression was detected in the posterior and anterior bulbs, in cells which anatomically correspond to MC and M2 neurons (Figure 7B). While LGC-57::GFP appeared to have overall low expression and little protein localisation could be seen above background (Figure 7C). LGC-58::GFP was clearly visible in the nerve ring and VC4/5, including some punctate structures (Figure 7D). Since these choline-sensitive members of the LGC-57 group showed little correlation with acetylcholine synapses, their diffuse protein localisation may be indicative of an extrasynaptic role (Figure 6C, Figure 7D).

Discussion

A Novel Family of Cholinergic LGICs

This study highlights the diversity among cholinergic LGICs in *C. elegans*. Nematodes have previously been shown to express acetylcholine and choline-gated excitatory LGICs related to nicotinic receptors, as well as inhibitory acetylcholine-gated chloride in the ACC group. Here we describe a second inhibitory subfamily, that contains channels gated by both choline and ACh: LGC-40, LGC-57 and LGC-58 (previously named GGR-1 and GGR-2). In contrast to the ACC group of acetylcholine-gated anion channels, these newly deorphanised channels are gated preferentially by choline, the metabolite of acetylcholine which is abundant at cholinergic synapses.

These results add to the already extensive catalogue of acetylcholine-gated channels in *C. elegans* (Putrenko et al., 2005; Takayanagi-Kiya et al., 2016), and to the growing number of choline-gated channels described in *C. elegans,* which previously consisted of the excitatory DEG-3/DES-2 channel found within the nAChR superfamily (Yassin et al., 2001). Together with our new data this highlights the expansion and importance of cholinergic transmission in nematodes. These newly deorphanised channels display subtle variations in their ability to bind ligands and antagonists, which translates into physiologically relevant differences that may increase the fine tuning in the control of neuronal transmission and contribute to complex neuronal signalling within a relatively minimal neuronal network. Interestingly, the electrophysiologically similar channels LGC-40, LGC-57, and LGC-58 show largely distinct patterns of expression within the nervous system of *C. elegans*, suggesting they may form homomeric channels with distinct functions *in vivo*. When tagged with a fluorescent protein, these three channels also showed a diffuse localisation pattern within the neuron, suggesting that in contrast to the ACC group channels, such as LGC-46 (Takayanagi-Kiya et al., 2016; Liu et al., 2017), these channels may not be synaptically localised. This suggests a possible distinct extrasynaptic role for choline by acting via these channels, in the modulation of the nervous system.

The observation that choline shows higher efficacy for these channels, a molecule generated at cholinergic synapses through catabolism of acetylcholine by cholinesterases, raises the possibility that choline is their true *in vivo* ligand and that choline itself may function as a neuromodulator. The idea that choline could activate cholinergic receptors differently from acetylcholine has been discussed for other cholinergic receptors that can be dose-dependently blocked or activated by choline (Purohit and Grosman, 2006). Here we have identified ionotropic cholinergic receptors in which choline act as a full agonist, showing preference in activation by choline over acetylcholine. Previous reports suggest

aromatic residues in the extracellular domain of mammalian neuromuscular AChRs play a vital part in stabilising the binding of acetylcholine over the binding to choline (Bruhova and Auerbach, 2017). Interestingly, although aromatic residues are present in the putative ligand binding regions of the *C. elegans* choline-gate channels identified in this study, their positions vary in comparison to mammalian AChRs (Figure 1-3). Specifically the LYS165-TYR210 hydrogen bond thought to be important in specifying acetylcholine over choline binding in mouse alpha 1 (*Chrna1*) (Bruhova and Auerbach, 2017) appears to be replaced with a hydrogen bond between ARG183 and TYR229 in LGC-57, which is conserved in both LGC-40 and LGC-58, in addition a further key tyrosine residue in mouse alpha 1 (TYR218) is replaced by tryptophan in all three choline-gated channels (Figure 1-3, 1-4). We also noted that none of the acetylcholine or choline activated channels characterised in this study contain the vicinal cysteine residues (Figure 1-3, 1-4) that are characteristic of nAChRs (Kao and Karlin, 1986). The regulation of choline concentrations in the context of acting as a neuromodulator in *C. elegans* is unclear, in mammals, studies have shown that reuptake of choline at the synapse may occur less than previously thought (Muramatsu et al., 2017), and the regulation of choline reuptake is highly plastic (Ferguson et al., 2004). Thus, it is not unreasonable to hypothesise that choline could be an authentic endogenous ligand for these channels *in vivo*.

A Polymodal LGIC Activated by Both Aminergic and Cholinergic Ligands

In this study we also identified a novel polymodal channel, LGC-39, which was gated not only by acetylcholine, but also by the aminergic ligands tyramine and octopamine. We observed dose-dependent activation of LGC-39 channels by these structurally distinct ligand classes of endogenous ligands at similar, physiologically relevant concentrations. Interestingly, while both cholinergic and non-cholinergic antagonists blocked the

acetylcholine induced response, only yohimbine, an α2 adrenergic receptor inhibitor, was able to block the octopamine induced response. Despite being an inhibitor of octopaminergic GPCRs in *C. elegans* (Packham et al., 2010), epinastine was not able to inhibit the octopamine induced response, instead it acted as an agonist both alone and in the presence of octopamine. It has previously been shown that strychnine acts as an agonist on mutant forms of α7 nAChRs in which residues contributing to acetylcholine binding were altered (Palma et al., 1999), it is possible that strychnine binds in a similar manner to wild-type LGC-39, thereby disrupting acetylcholine activation but not octopamine activation, suggesting acetylcholine and octopamine have different binding modes.

The expression pattern of *lgc-39* suggests that the channel might be exposed to all these ligands *in vivo*; for example, *lgc-39* is highly expressed in the AVA premotor neurons, which receive a large amount of input from acetylcholine producing neurons (White, 1986), as well as from the RIC neurons, the only octopamine producing cells in the *C. elegans* nervous system (Alkema et al., 2005). The AVA neurons also receive some input from tyraminergic and dopaminergic neurons, transmitters which we also found can activate LGC-39. Interestingly, in contrast to the choline-gated channels LGC-40, LGC-57, and LGC-58, we observe clear punctate localisation of LGC-39 in both the nerve ring and along the ventral cord, with no fluorescence visible in the cell bodies. This may suggest a role for LGC-39 as postsynaptic receptor for both cholinergic and aminergic neurotransmission.

The concept of a truly polymodal ionotropic receptor, that can be activated by structurally diverse compounds, has not before been investigated in great detail, though previous observations have described roles for receptors that can use dual ligands for allosteric modulation (Cummings and Popescu, 2015). For example, dopamine exhibits a pseudo competitive ability to antagonise $GABA_A$ currents, although this effect cannot be blocked by competitive $GABA_A$ antagonists, which bind the main binding pocket (Hoerbelt

et al., 2015). Further, D-serine has been shown to function as an allosteric modulator of NMDA receptor activity (Wolosker and Balu, 2020). In contrast to these examples, based on their capability to achieve dose-dependent activation by both amines and acetylcholine, both groups of neurotransmitters appear to be true ligands of LGC-39, most likely interacting with the ligand-binding domain. Understanding the mechanisms by which these multiple neurotransmitters can activate LGC-39 and potentially affect different behavioural outputs will be of interest in future studies.

Functional Insights into The *C. elegans* Connectome

With increasing molecular and physiological characterisation of neurotransmitter receptors in *C. elegans*, it is becoming feasible to predict the functionality of synapses more accurately in the *C. elegans* connectome. In this study we used the expression pattern of newly and previously deorphanised LGICs for the three classical neurotransmitters, acetylcholine, glutamate, and GABA, to predict the polarity of synapses in the *C. elegans* connectome. By assigning synapse polarity based on relative expression levels of anionic and cationic receptors, we have provisionally predicted the sign of chemical synapses involving classical neurotransmitters. Although similar attempts to assign polarity to *C. elegans* synapses have been made in the past (Fenyves et al., 2020), these predictions were based upon incomplete or incorrect ligand assignment for many LGICs, for example *ggr-1 (lgc-57), ggr-2 (lgc-58)* and *ggr-3 (lgc-56)* were listed as anionic GABA receptors, which we have subsequently have shown are gated by choline and acetylcholine for *lgc-57* and *lgc-58* and monoamines for *lgc-56* (Morud et al., 2021). Our revised predictions correlate well with experimental data for many well-characterised circuits, such as the excitatory connections between the ASH nociceptors and the AVA interneurons, as well as between the AVAs and the VA and DA motorneurons (Mellem et al., 2002; Piggott et al., 2011). Our predicted

617 inhibitory connection between AVB and AVA interneurons also correspond well with
618 empirical data on the locomotor circuit (Kawano et al., 2011; Qi et al., 2012). In addition to
619 providing sign predictions for synaptic connections, our model also provides a ratio of
620 excitatory to inhibitory expression for each neuronal class and neurotransmitter. Not only do
621 our predictions generate interesting functional hypotheses for future investigation, but this
622 additional information also allows these predictions to be critically assessed. It also raises the
623 question whether these connections, with low receptor ratios, represent truly complex
624 connections, a question that could be addressed in future studies.

625 A surprising outcome of the expression analysis was the high frequency with which
626 individual neurons expressed cationic and anionic receptors for the same neurotransmitter.
627 This was especially prevalent for acetylcholine; our analysis indicated that 60% of neural
628 classes express both inhibitory and excitatory ionotropic receptors for acetylcholine, 30% for
629 glutamate and 10% for GABA. One explanation for this apparent paradox is that excitatory
630 and inhibitory ionotropic receptors might be differentially localised in neurons, with some
631 found extrasynaptically and others enriched in synapses. Various *C. elegans* LGICs are
632 known to act in regions other than the post-synapse; for example, *lgc-35* has been shown to
633 mediate GABA spill-over transmission (Jobson et al., 2015), while *lgc-46* appears be
634 localised to both pre-synapses (Takayanagi-Kiya et al., 2016) and post-synapses (Liu et al.,
635 2017). The choline-sensitive channels from the LGC-57 group likewise appear to be extra
636 synaptic in their localisation (Figure 7). In addition, postsynaptic sites might themselves
637 contain a mixture of excitatory and inhibitory ionotropic receptors, which could differ in their
638 ligand affinity, desensitisation kinetics and regulation. Indeed, LGIC localisation is not static;
639 for example, glutamatergic AMPA receptors have been shown in many species to increase
640 their synaptic localisation during learning (Malinow and Malenka, 2002), and recent evidence
641 indicates that *C. elegans* LGICs also display regulated membrane trafficking upon learning

(Morud et al., 2021). Thus, *C. elegans* may contain large numbers of complex cholinergic synapses with the potential to be excitatory or inhibitory depending on context or experience.

Author Contributions

I.H., J.M. and W.R.S. designed the experiments. I.H., J.M., and A.C. performed experiments and analysed data. I.H., J.M. and W.R.S. wrote the manuscript and all authors read and critically revised the manuscript to its final form.

Acknowledgements

We would like to acknowledge Denise Walker for assistance in cloning and the construction and maintenance of strains, as well as other past and present members of the Schafer lab for helpful discussions. We would also like to acknowledge the Centre for Cellular Imaging at the University of Gothenburg and the Swedish National Microscopy Infrastructure, Sweden, for providing light microscopy facilities. This work was supported by grants from the Medical Research Council (MC-A023-5PB91), the Wellcome Trust (WT103784MA), the Research Foundation-Flanders (G079521N) and the National Institutes of Health (R01NS110391) (WRS). As well as the Swedish Research council (2017-00236), Knut och Alice Wallenbergs foundation (KAW2019,0293), Magnus Bergvalls stiftelse and Åke Wibergs stiftelse (J.M.)

References

Alkema MJ, Hunter-Ensor M, Ringstad N, Horvitz HR (2005) Tyramine functions independently of octopamine in the Caenorhabditis elegans nervous system. Neuron 46.

666 Barbagallo B, Prescott HA, Boyle P, Climer J, Francis MM (2010) A dominant mutation in a
667 neuronal acetylcholine receptor subunit leads to motor neuron degeneration in
668 Caenorhabditis elegans. J Neurosci 30.
669 Bondarenko V, Targowska-Duda KM, Jozwiak K, Tang P, Arias HR (2014) Molecular
670 interactions between mecamylamine enantiomers and the transmembrane domain of the
671 human α4β2 nicotinic receptor. Biochemistry 53.
672 Brams M, Pandya A, Kuzmin D, van Elk R, Krijnen L, Yakel JL, Tsetlin V, Smit AB, Ulens
673 C (2011) A structural and mutagenic blueprint for molecular recognition of strychnine
674 and d-tubocurarine by different Cys-loop receptors. PLoS Biol 9.
675 Bruhova I, Auerbach A (2017) Molecular recognition at cholinergic synapses: acetylcholine
676 versus choline. J Physiol 595.
677 Cattoni DI, Chara O, Kaufman SB, Flecha FLG (2015) Cooperativity in binding processes:
678 New insights from phenomenological modeling. PLoS One 10.
679 Chalfie M, Sulston JE, White JG, Southgate E, Nichol Thomson J, Brenner S (1985) The
680 neural circuit for touch sensitivity in Caenorhabditis elegans. J Neurosci 5.
681 Cully DF, Paress PS, Liu KK, Schaeffer JM, Arena JP (1996) Identification of a Drosophila
682 melanogaster glutamate-gated chloride channel sensitive to the antiparasitic agent
683 avermectin. J Biol Chem.
684 Cully DF, Vassilatis DK, Liu KK, Paress PS, Van Der Ploeg LHT, Schaeffer JM, Arena JP
685 (1994) Cloning of an avermectin-sensitive glutamate-gated chloride channel from
686 Caenorhabditis elegans. Nature.
687 Cummings KA, Popescu GK (2015) Glycine-dependent activation of NMDA receptors. J
688 Gen Physiol 145.
689 Dickinson D, Slabodnick M, Chen A, Goldstein B (2018) SapTrap assembly of repair
690 templates for Cas9-triggered homologous recombination with a self-excising cassette.

691 microPublication Biol 2018.
692 Faumont S, Lindsay TH, Lockery SR (2012) Neuronal microcircuits for decision making in
693 C. elegans. Curr Opin Neurobiol 22.
694 Fenyves BG, Szilágyi GS, Vassy Z, Sőti C, Csermely P (2020) Synaptic polarity and sign-
695 balance prediction using gene expression data in the Caenorhabditis elegans chemical
696 synapse neuronal connectome network. PLoS Comput Biol 16.
697 Ferguson SM, Bazalakova M, Savchenko V, Tapia JC, Wright J, Blakely RD (2004) Lethal
698 impairment of cholinergic neurotransmission in hemicholinium-3-sensitive choline
699 transporter knockout mice. Proc Natl Acad Sci U S A 101.
700 Gisselmann G, Pusch H, Hovemann BT, Hatt H (2002) Two cDNAS coding for histamine-
701 gated ion channels in D. melanogaster. Nat Neurosci.
702 Halevi S, McKay J, Palfreyman M (2002) The C.elegans ric-3 gene is required for maturation
703 of nicotinic acetylcholine receptors. EMBO J 21.
704 Hobert O (2013) The neuronal genome of Caenorhabditis elegans. WormBook.
705 Hoerbelt P, Lindsley TA, Fleck MW (2015) Dopamine directly modulates GABAA
706 receptors. J Neurosci 35.
707 Jobson MA, Valdez CM, Gardner J, Garcia LR, Jorgensen EM, Beg AA (2015) Spillover
708 transmission is mediated by the excitatory GABA receptor LGC-35 in C. elegans. J
709 Neurosci.
710 Jones AK, Davis P, Hodgkin J, Sattelle DB (2007) The nicotinic acetylcholine receptor gene
711 family of the nematode Caenorhabditis elegans: An update on nomenclature. Invertebr
712 Neurosci 7.
713 Jones AK, Sattelle DB (2008) The cys-loop ligand-gated ion channel gene superfamily of the
714 nematode, Caenorhabditis elegans. Invertebr Neurosci 8:41–47 Available at:
715 http://link.springer.com/10.1007/s10158-008-0068-4.

716 Jumper J et al. (2021) Highly accurate protein structure prediction with AlphaFold. Nature
717 596.
718 Kao PN, Karlin A (1986) Acetylcholine receptor binding site contains a disulfide cross-link
719 between adjacent half-cystinyl residues. J Biol Chem 261.
720 Karim N, Wellendorph P, Absalom N, Johnston GAR, Hanrahan JR, Chebib M (2013)
721 Potency of GABA at human recombinant GABAA receptors expressed in Xenopus
722 oocytes: A mini review. Amino Acids 44.
723 Kawano T, Po MD, Gao S, Leung G, Ryu WS, Zhen M (2011) An imbalancing act: Gap
724 junctions reduce the backward motor circuit activity to bias C. elegans for forward
725 locomotion. Neuron 72.
726 Kirsch J (2006) Glycinergic transmission. Cell Tissue Res 326.
727 Kondo M, Nakamura Y, Ishida Y, Yamada T, Shimada S (2014) The 5-HT3A receptor is
728 essential for fear extinction. Learn Mem 21.
729 Liu P, Chen B, Mailler R, Wang ZW (2017) Antidromic-rectifying gap junctions amplify
730 chemical transmission at functionally mixed electrical-chemical synapses. Nat Commun.
731 Lombaert N, Hennes M, Gilissen S, Schevenels G, Aerts L, Vanlaer R, Geenen L, Van
732 Eeckhaut A, Smolders I, Nys J, Arckens L (2018) 5-HTR 2A and 5-HTR 3A but not 5-
733 HTR 1A antagonism impairs the cross-modal reactivation of deprived visual cortex in
734 adulthood. Mol Brain 11.
735 Malinow R, Malenka RC (2002) AMPA receptor trafficking and synaptic plasticity. Annu
736 Rev Neurosci 25:103–126.
737 Margie O, Palmer C, Chin-Sang I (2013) C. elegans chemotaxis assay. J Vis Exp.
738 Mellem JE, Brockie PJ, Zheng Y, Madsen DM, Maricq A V. (2002) Decoding of polymodal
739 sensory stimuli by postsynaptic glutamate receptors in C. elegans. Neuron 36.
740 Morud J, Hardege I, Liu H, Wu T, Choi M-K, Basu S, Zhang Y, Schafer WR (2021)

741 Deorphanization of novel biogenic amine-gated ion channels identifies a new serotonin
742 receptor for learning. Curr Biol.
743 Muramatsu I, Uwada J, Masuoka T, Yoshiki H, Sada K, Lee KS, Nishio M, Ishibashi T,
744 Taniguchi T (2017) Regulation of synaptic acetylcholine concentrations by
745 acetylcholine transport in rat striatal cholinergic transmission. J Neurochem 143.
746 Packham R, Walker RJ, Holden-Dye L (2010) The effect of a selective octopamine
747 antagonist, epinastine, on pharyngeal pumping in Caenorhabditis elegans. Invertebr
748 Neurosci 10.
749 Palma E, Fucile S, Barabino B, Miledi R, Eusebi F (1999) Strychnine activates neuronal α7
750 nicotinic receptors after mutations in the leucine ring and transmitter binding site
751 domains. Proc Natl Acad Sci U S A 96.
752 Pereira L, Kratsios P, Serrano-Saiz E, Sheftel H, Mayo AE, Hall DH, White JG, LeBoeuf B,
753 Garcia LR, Alon U, Hobert O (2015) A cellular and regulatory map of the cholinergic
754 nervous system of C. Elegans. Elife 4.
755 Piggott BJ, Liu J, Feng Z, Wescott SA, Xu XZS (2011) The neural circuits and synaptic
756 mechanisms underlying motor initiation in C. elegans. Cell 147.
757 Pirri JK, McPherson AD, Donnelly JL, Francis MM, Alkema MJ (2009) A Tyramine-Gated
758 Chloride Channel Coordinates Distinct Motor Programs of a Caenorhabditis elegans
759 Escape Response. Neuron 62.
760 Purohit Y, Grosman C (2006) Block of muscle nicotinic receptors by choline suggests that
761 the activation and desensitization gates act as distinct molecular entities. J Gen Physiol
762 127.
763 Putrenko I, Zakikhani M, Dent JA (2005) A family of acetylcholine-gated chloride channel
764 subunits in Caenorhabditis elegans. J Biol Chem 280.
765 Qi YB, Garren EJ, Shu X, Tsien RY, Jin Y (2012) Photo-inducible cell ablation in

766 Caenorhabditis elegans using the genetically encoded singlet oxygen generating protein
767 miniSOG. Proc Natl Acad Sci U S A 109.
768 Raizen DM, Lee RYN, Avery L (1995) Interacting genes required for pharyngeal excitation
769 by motor neuron MC in Caenorhabditis elegans. Genetics 141.
770 Rakowski F, Karbowski J (2017) Optimal synaptic signaling connectome for locomotory
771 behavior in Caenorhabditis elegans: Design minimizing energy cost. PLoS Comput Biol
772 13.
773 Ranganathan R, Cannon SC, Horvitz HR (2000) MOD-1 is a serotonin-gated chloride
774 channel that modulates locomotory behaviour in C. elegans. Nature 408.
775 Ringstad N, Abe N, Horvitz HR (2009) Ligand-gated chloride channels are receptors for
776 biogenic amines in C. Elegans. Science (80-) 325.
777 Schwartz ML, Jorgensen EM (2016) SapTrap, a toolkit for high-throughput CRISPR/Cas9
778 gene modification in Caenorhabditis elegans. Genetics 202.
779 Shannon P, Markiel A, Ozier O, Baliga NS, Wang JT, Ramage D, Amin N, Schwikowski B,
780 Ideker T (2003) Cytoscape: A software Environment for integrated models of
781 biomolecular interaction networks. Genome Res 13.
782 Stiernagle T (2006) Maintenance of C. elegans. WormBook.
783 Takayanagi-Kiya S, Zhou K, Jin Y (2016) Release-dependent feedback inhibition by a
784 presynaptically localized ligand-gated anion channel. Elife.
785 Taylor SR et al. (2021) Molecular topography of an entire nervous system. Cell 184.
786 Tyzio R, Holmes GL, Ben-Ari Y, Khazipov R (2007) Timing of the developmental switch in
787 GABAA mediated signaling from excitation to inhibition in CA3 rat hippocampus using
788 gramicidin perforated patch and extracellular recordings. In: Epilepsia.
789 van Giesen L, Kilian PB, Allard CAH, Bellono NW (2020) Molecular Basis of Chemotactile
790 Sensation in Octopus. Cell.

791 White JG. (1986) The structure of the nervous system of the nematode Caenorhabditis
792 elegans. Philos Trans R Soc London B, Biol Sci 314:1–340.
793 Wolosker H, Balu DT (2020) d-Serine as the gatekeeper of NMDA receptor activity:
794 implications for the pharmacologic management of anxiety disorders. Transl Psychiatry
795 10.
796 Wotring VE, Miller TS, Weiss DS (2003) Mutations at the GABA receptor selectivity filter:
797 A possible role for effective charges. J Physiol 548.
798 Yassin L, Gillo B, Kahan T, Halevi S, Eshel M, Treinin M (2001) Characterization of the
799 DEG-3/DES-2 receptor: A nicotinic acetylcholine receptor that mutates to cause
800 neuronal degeneration. Mol Cell Neurosci 17.
801 Yemini E, Lin A, Nejatbakhsh A, Varol E, Sun R, Mena GE, Samuel ADT, Paninski L,
802 Venkatachalam V, Hobert O (2020) NeuroPAL: A Multicolor Atlas for Whole-Brain
803 Neuronal Identification in C. elegans. Cell.
804

805 ## Main Figure Legends

806 **Figure 1. Deorphanisation of Cholinergic Ligand-Gated Ion Channels.** (**A**) Simplified phylogenetic tree of
807 subgroups of pentameric ligand-gated ion channels in *C. elegans*, groups of interest are highlighted by colour:
808 'ACC' group of ACh-gated channels (red), LGC-45 group (yellow), LGC-41 group (blue), LGC-57 group
809 (green). Triangles represent collapsed isoforms/families, dots represent genes with a single isoform, branch
810 lengths are not to scale, see Figure 1-1 for full expanded phylogenetic tree. (**B**) Continuous current traces of
811 *Xenopus* oocytes expressing LGC-40, LGC-57, LGC-58, and LGC-49, oocytes were perfused for 10s with a
812 selection of a panel of ligands each at 1mM: ACh (acetylcholine), Ch (choline), Bet (betaine), Tyr (tyramine),
813 DA (dopamine), 5-HT (serotonin), Oct (octopamine), GABA, Glu (glutamate), His (histamine), MA
814 (melatonin), see Figure 1-2 for additional traces and ligands. (**C**) Dose response curves for LGC-40, LGC-57,
815 LGC-58, and LGC-49 in response to their major ligand(s). Current is normalised by I/Imax for each oocyte, for
816 LGC-49 the current is presented as raw un-normalised current due to difficulties with repeated ligand
817 applications for this specific channel. Error bars represent SEM of 5-14 oocytes. Curves are fitted with a four-

parameter variable slope, inserts show EC_{50} in µM for each ligand. Hillslope values: LGC-40: ACh:1.4, Ch:2.1, LGC-57: ACh: 1.4, Ch: 1.8, LGC-58: ACh: 2.4, Ch: 2.0. See Figure 1-2 and 1-6 for additional TEVC traces and alignments, Figure 1-3, and Figure 1-4 for alignment of the ligand binding loops and Figure 1-5 for representative dose response traces. See Table 1-1 for a summary of all channels and ligands tested in this study.

Figure 2. Ion Selectivity and Antagonistic Characterisation of Cholinergic LGICs. (A) Representative current voltage plots of newly deorphanised channels in ND96, Na^+ gluconate or NMDG solutions. Current was normalised by leak current subtraction (in absence of activating ligand) and the peak current for each oocyte. (**B**) Tukey's box plot of ΔE_{rev} of NMDG and Na^+ Gluconate vs. ND96 in oocytes expressing LGC-40, LGC-57, LGC-58, LGC-46, and LGC-49, E_{rev} was calculated in the presence of the primary agonist of each channel and leak subtracted. N=6-11 oocytes. (**C**) Antagonist application in the presence of ligands using mecamylamine, strychnine and tubocurarine. Current was normalised by I/Imax for each oocyte, curves are fitted with a three-parameter variable slope, error bars represent SEM of 2-7 oocytes, inserts show IC_{50} in µM for each antagonist. (**D & F**) Representative traces of oocytes expressing LGC-40, LGC-57, LGC-58, LGC-46, or LGC-49 undergoing repeated agonist application (20 µM choline for LGC-40, LGC-57, and LGC-58, 70 µM and 20 µM acetylcholine for LGC-46 and LGC-49 respectively) with 10s, 30s and 60s wash intervals in ND96. (**E & G**) Quantification of repeated agonist stimulation, mean current ratio of oocytes at each wash interval is plotted. Error bars represent SEM. N=5-9 oocytes per condition. See Figure 2-1 for representative antagonist dose response traces.

Figure 3. LGC-39 Forms a Polymodal Ligand-Gated Ion Channel. (**A**) Continuous current trace of a *Xenopus* oocyte clamped at -60mV expressing LGC-39, perfused during 10s pulses with a panel of ligands each at 1mM: Ach (acetylcholine), Ch (choline), Bet (betaine), Tyr (tyramine), DA (dopamine), 5-HT (serotonin), Oct (octopamine), GA (GABA), Glu (glutamate), His (histamine). (**B**) Dose response curve for LGC-39 in response to ACh, Oct, and Tyr. Current is normalised by I/Imax (Imax at 3 mM agonist) for each oocyte and each compound (dose responses for different agonists could not be done within the same oocytes for technical reasons). Error bars represent SEM of 8-12 oocytes. Curves are fitted using a four-parameter variable slope, inserts show EC_{50} in µM for each ligand. Hillslope values: Tyr: 1.79, Oct: 1.43 and ACh: 1.96. (**C**) Current-voltage relationship during recordings in NMDG, Na^+ Gluconate or ND96 in oocytes expressing LGC-39. Insert shows ΔE_{rev} vs. ND96 in mV +/- SEM of 5 oocytes. (**D-E**) Antagonist dose response curves for LGC-39

848 expressing oocytes activated by either ACh, Oct or no ligand at a constant dose and varying the antagonist doses
849 (mecamylamine, strychnine, epinastine and yohimbine). Error bars represent SEM of 3-7 oocytes. Current is
850 normalised by I/Imax, where Imax is the lowest antagonist dose. Curves are fit with a three-parameter variable
851 slope, inserts show IC_{50} (**D**) or EC_{50} (**E**) in μM for each ligand. (**F**) Three different agonists do not differ in how
852 they influence the ability for LGC-39 to be stimulated with short time intervals after repeated stimulation. See
853 Figure 2-1 for representative antagonist dose response traces.
854
855 **Figure 4. Newly Deorphanised LGICs are Expressed Broadly in the Nervous System. (A-E)** Fluorescent
856 reporters of intercistonically spliced mKate2 or GFP driven under the promoter and/or genomic sequence of
857 reveals broad neuronal expression of cholinergic channels with little overlap. *lgc-40* expression was identified in
858 OLQs, BAG, M2, MC, ALM, PVM and PLM. *lgc-57* expression was identified in M3, RIP, URY, AIB, RMH,
859 SMB, ADA, ventral cord neurons and PVR. *lgc-58* expression was identified in I3, IL1, CEPs, URA, URB,
860 SIA, ADE, RIS, RMG, VC3-6, PVQ and PHC. *lgc-49* expression was identified in CEPs, URX, AFD, ASJ,
861 RIG, PVQ, PVC, PLN and ALN. *lgc-39* expression was identified in URB, RIA, AVA, AVD, M1, AQR, AVK,
862 AS, VA and DA. (**F**) Schematic depicting a subset of the synaptic connections received by the *lgc-39* expressing
863 neuron class, AVA, numbers in brackets show the total number of synapses for each connection. See Figure 4-1
864 for cell ID of still orphan LGCs. See Table 4-1 for strain list, 4-2 for primer list, 4-3 expression overlap
865 compared with the CeNGEN dataset.
866
867 **Figure 5. Predicting Synapse Polarity Based on LGIC Expression.** (**A**) Bar chart and table depicting the
868 percentage of total neuron classes expression inhibitory, excitatory, both or no ionotropic receptors for GABA,
869 glutamate (Glu) and acetylcholine (ACh). (**B**) Bar chart and table depicting the percentage of total synapses for
870 a given neurotransmitter that are predicted to be inhibitory, excitatory or have no prediction. (**C**) Network
871 diagram depicting the polarity of synaptic connections between neural classes, connection colour show polarity:
872 teal (inhibitory), pink (excitatory), grey (no prediction). Gap junctions are represented in dashed lines. Line
873 weight represents number of synapses and nodes are coloured by the major neurotransmitter a class release.
874 Diagram made with cytoscape using the EntOpt clustering package. (**D**) Network diagram depicting the
875 predicted polarity of the locomotion circuit, connection colour shows polarity: teal (inhibitory), pink
876 (excitatory), grey (no prediction). Inserts next to each neuron node show the fold magnitude of expression of the
877 major receptor type for each neurotransmitter in each neural class, e.g., AVA neurons express 1.3x as many

inhibitory ACh receptors than excitatory and 8.9x as many excitatory glutamate receptors than inhibitory. Gap junctions are represented by dashed lines. Line weight represents number of synapses and nodes are coloured by the major neurotransmitter a class release. Diagram made with cytoscape. See Figure 5-1 for binary polarity predictions for each neuronal class and 5-2 for expression heatmap of the 3 major neurotransmitters. See Table 5-1 for list of LGC ligands.

Figure 6. Correlation of Cholinergic Synapses with Expression Pattern of Cholinergic Ion Channels. (**A-B**) Heatmaps showing the expression level of newly deorphanised LGICs in each neural class. Neurons are sorted by the total number of cholinergic synapses they receive (top, 'Incoming') or make (bottom, 'Outgoing'). (**C & D**) Scatter plots showing correlation between the total number of incoming (red) or outgoing (orange) cholinergic synapses for a given neuronal class and expression of *lgc-46, lgc-57, lgc-58, lgc-40,* and *lgc-39*. See Figure 6-1 for correlation graphs of remaining LGCs from this study.

Figure 7. Protein expression pattern of cholinergic ion channels. (**A-D**) Localisation of endogenously GFP tagged LGC-39, LGC-40, LGC-57, and LGC-58. White arrows highlight areas of interest, represented in higher magnification below. See Figure 7-1 for dose response traces for GFP tagged channels.

Extended Data Legends

Tables

Table 1-1: **Overview of LGICs and LGIC combinations screened in this study, including agonists/antagonists and selectivity information.** Groups are highlight by colour: 'ACC' group of ACh-gated channels (red), LGC-45 group (yellow), LGC-41 group (blue), LGC-57 group (green).

Table 4-1: **List of *C. elegans* strains used in this study**

Table 4-2: **List of primers used in this study**

Table 4-3: **Expression overlap between fluorescent reporter strains and CeNGEN RNAseq expression data.**

Table 5-1: **The list shows ligand identity and ion selectivity for LGICs in *C. elegans*.** Each gene is assigned a polarity based upon its ion selectivity, this is shown in column 'Pos/Neg' as P: positive (cation selectivity) or N:

negative (anion selectivity). For orphan receptors the ligand and ion selectivity has been predicted based on homology, this has been noted in the column 'Inferred' as 'yes'. The references where the receptor has a validated ligand are from experiments evaluating receptors using electrophysiological characterisation in a heterologous expression system.

Figures

Extended Data Figures

Figure 1-1: **Full phylogenetic tree.** Reproduced from (Morud et al., 2021). Generated with PHYLIP Neighbour Joining, not to scale.

Figure 1-2: **Negative traces for still orphan and characterised LGICs.** A-F, H. Continuous TEVC traces from oocytes clamped at -60mV expressing LGICs, exposed to 10s of a selection of a panel of ligands. Acetylcholine (ACh), choline (Ch), dopamine (DA), betaine (Bet), tyramine (Tyr), serotonin (5-HT), octopamine (Oct), GABA, glutamate (Glu), glycine (Gly), histamine (His), melatonin (MA). E. Co-expression of LGC-48 and ACC-4, nor LGC-48 on its own, did not show any agonist-induced current by the ligands tested. F. Continuous TEVC traces from oocytes clamped at -60mV expressing LGC-47, ACC-1, or a combination, exposed to 10 s of a panel of ligands. Note that the small changes in current seen in the traces are attributed to recording and perfusion artefacts G. ACh-induced dose response curves for oocytes expressing ACC-1 alone, or in combination with LGC-47. Error bars represent SEM of 7-12 oocytes per construct, insert shows EC_{50} values. H. Continuous TEVC traces from oocytes clamped at -60 mV expressing LGC-39 exposed to 10 s of a panel of ligands. Note that the small changes in current seen in the traces are attributed to recording and perfusion artefacts.

Figure 1-3: ***C. elegans* choline-gated channels show differences in the position of key aromatic residues in the ligand binding domain.** A. Alignment of PAR motifs for channels in the diverse and ACC groups. B. Alignment of mouse chrna1 (uniprot ID: P04756) and *C. elegans lgc-40, lgc-57,* and *lgc-58*. Red stars highlight key ligand binding residues from mouse *Chrna1* as described in (Bruhova and Auerbach, 2017), blue stars highlight the vicinal cysteines of mouse CHRNA1. C. Predicted AlphaFold (Jumper et al., 2021) structures of the ligand binding domains from CHRNA1 (AF-P04756-F1) and LGC-57 (AF-Q09453-F1).

Figure 1-4: **Full alignments of a selection of C. elegans pentameric ligand gated ion channels and mouse *Chrna1*.** Generated with CLUSTAL omega, colour applied with CLUSTAL formatting.

Figure 1-5: **Representative traces of different doses during dose response experiments for all characterised channels in this study.** Black bars show agonist application time of either 7 s or 10 s. Acetylcholine (ACh), octopmaine (Oct), tyramine (Tyr).

Figure 1-6: **Still orphan LGICs co-expressed with RIC-3.** A. Representative traces oocytes expressing RIC-3 alone or in combination with LGC-42, LGC-44, LGC-45, LGC-47, and LGC-48. Oocytes were exposed to a 10 s perfusion (indicated by the black bar) of selection of a panel of ligands. B. Quantification of peak current induced after perfusing at 1mM of acetylcholine, choline, and betaine.

Figure 2-1: **Representative traces during different antagonist applications.** Each channel was exposed to its primary ligand at EC_{50} along with an increasing antagonist concentration. Black bars above the trace show agonist/antagonist application time of 7 s.

Figure 4-1: **Expression patterns of still orphan LGICs and LGC-46 characterisation.** A-B. Expression of fluorescent reporters for still orphan LGCIs, head body and tail are shown for *lgc-42* and *lgc-47* (A), head only is shown for *lgc-43*, *lgc-45,* and *lgc-48* (B). C. Continues recording trace for LGC-46 and the ACh-induced dose response curve for LGC-46. Error bars represent SEM of 6 oocytes. Insert shows EC_{50}. D. Expression of fluorescent reporters for lgc-46p shows a broad neuronal expression pattern with expression in e.g., AIZ, RIH and AVE neurons.

Figure 5-1: **Binary heatmap of synaptic sign prediction for the three major neurotransmitters; ACh, glutamate and GABA.** The heatmap shows the summed expression level of all LGICs in *C. elegans* per neural class and neurotransmitter, a net sum of excitatory channels is displayed in red, inhibitory in green, equal expression in peach and no expression of LGICs in white.

Figure 5-2: **Expression heatmap for the three major neurotransmitters.** The heatmap shows the summed expression level, and ion selectivity, for LGICs separated by transmitter (ACh, glutamate (Glu) and GABA) and neural class. Net excitatory channel expression is represented in pink and inhibitory in green.

Figure 6-1: **Correlation graphs between cholinergic synapses and expression of selected LGICs.** Scatter plots showing gene expression level vs total number of incoming cholinergic synapses (red) and outgoing cholinergic synapses (orange). Lines fit using relplot with shaded areas representing the standard error of the line fit.

Figure 7-1: **GFP tagging of LGICs does not influence channel function.** ACh- or choline-induced dose response curves for oocytes expressing GFP tagged versions of LGC-40, LGC-57 and LGC-58 shows that EC_{50}

966 values are not influenced by the insertion of the GFP tag. Error bars represent SEM of 7-12 oocytes per
967 construct, insert shows EC_{50} values.

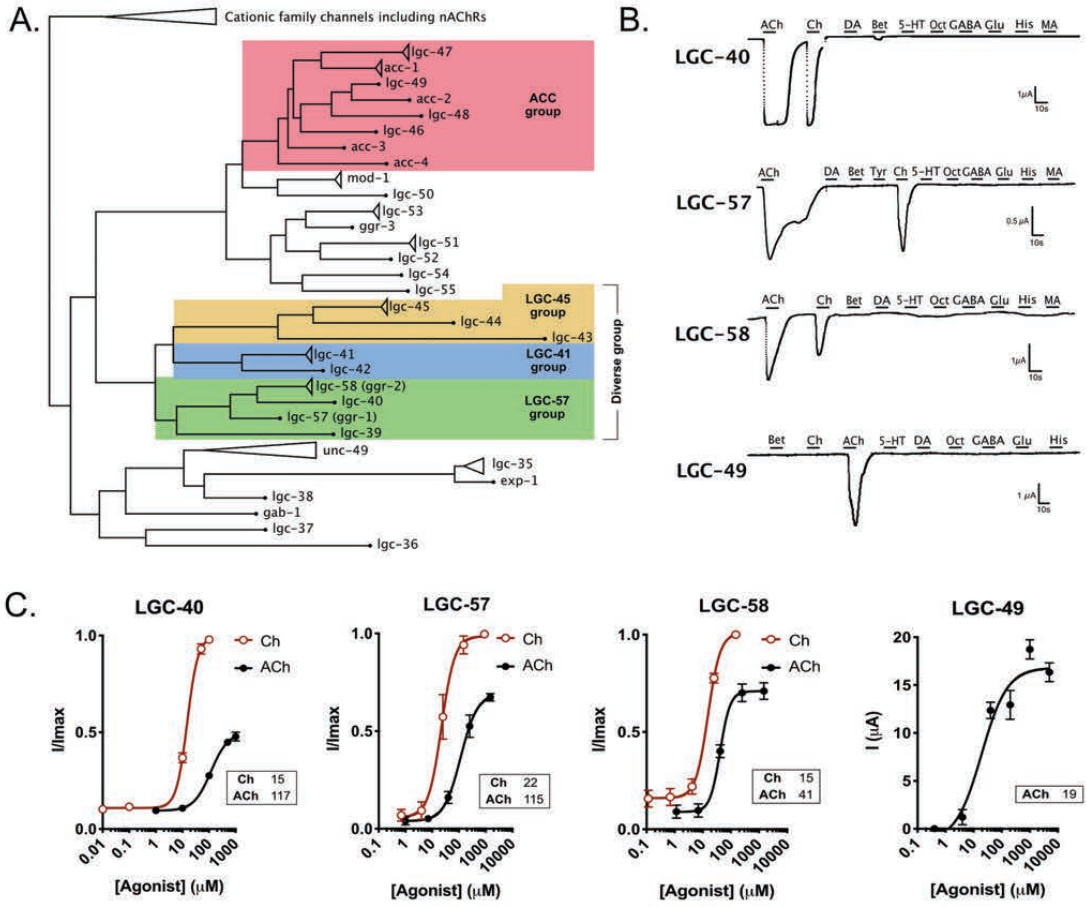

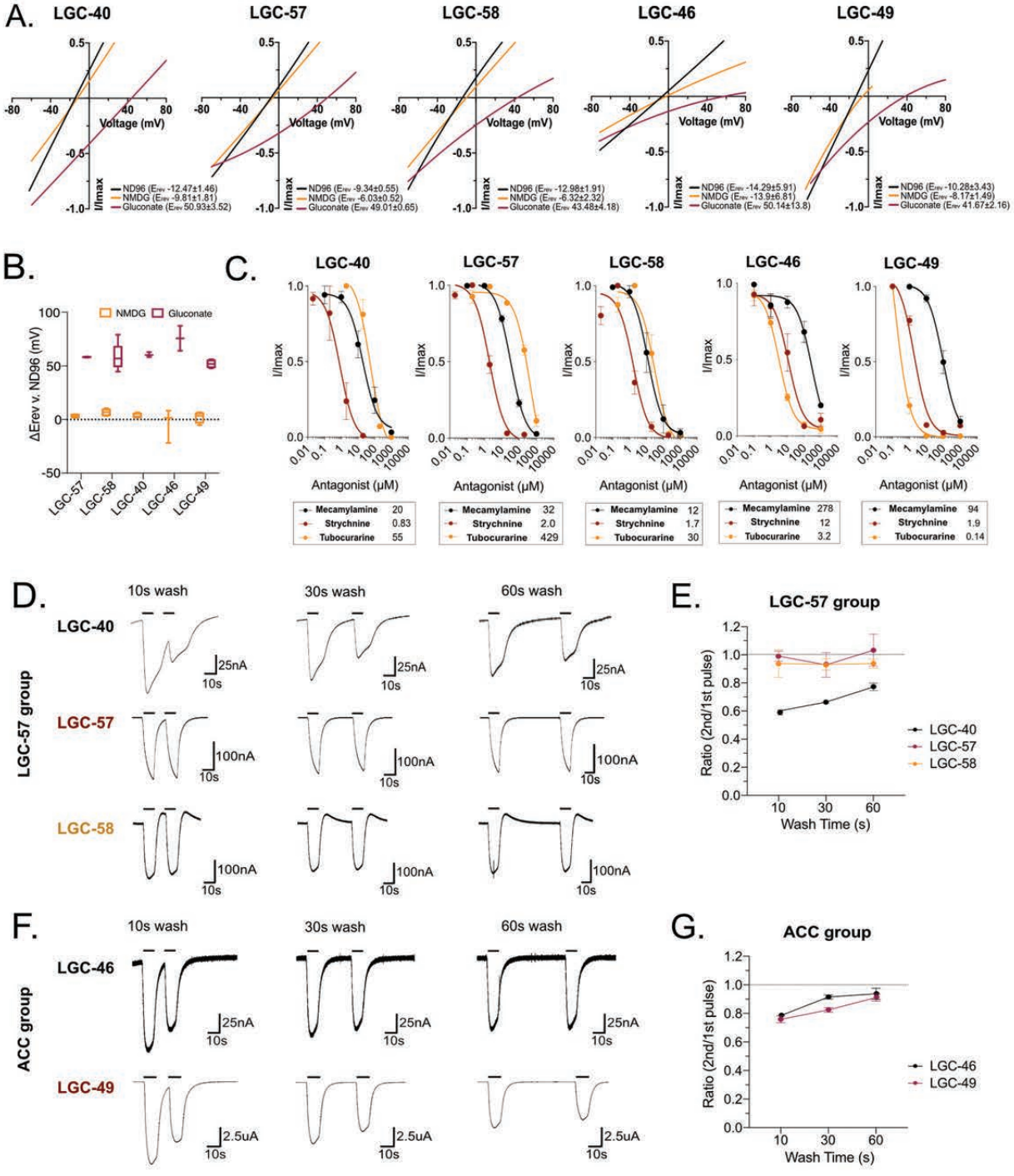

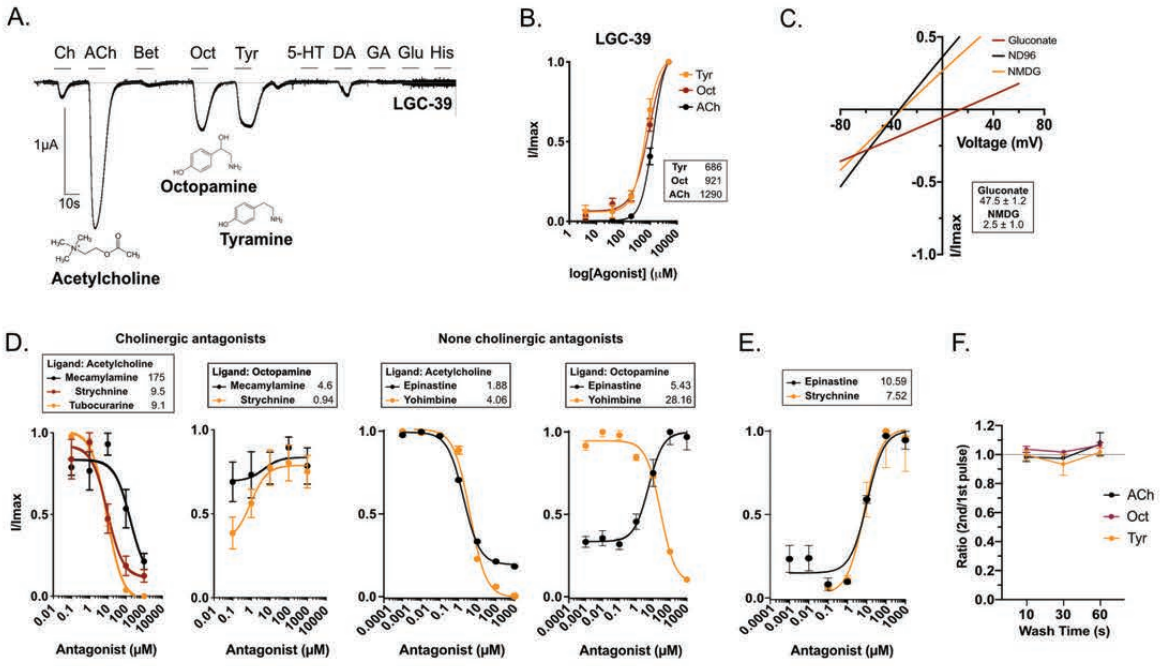

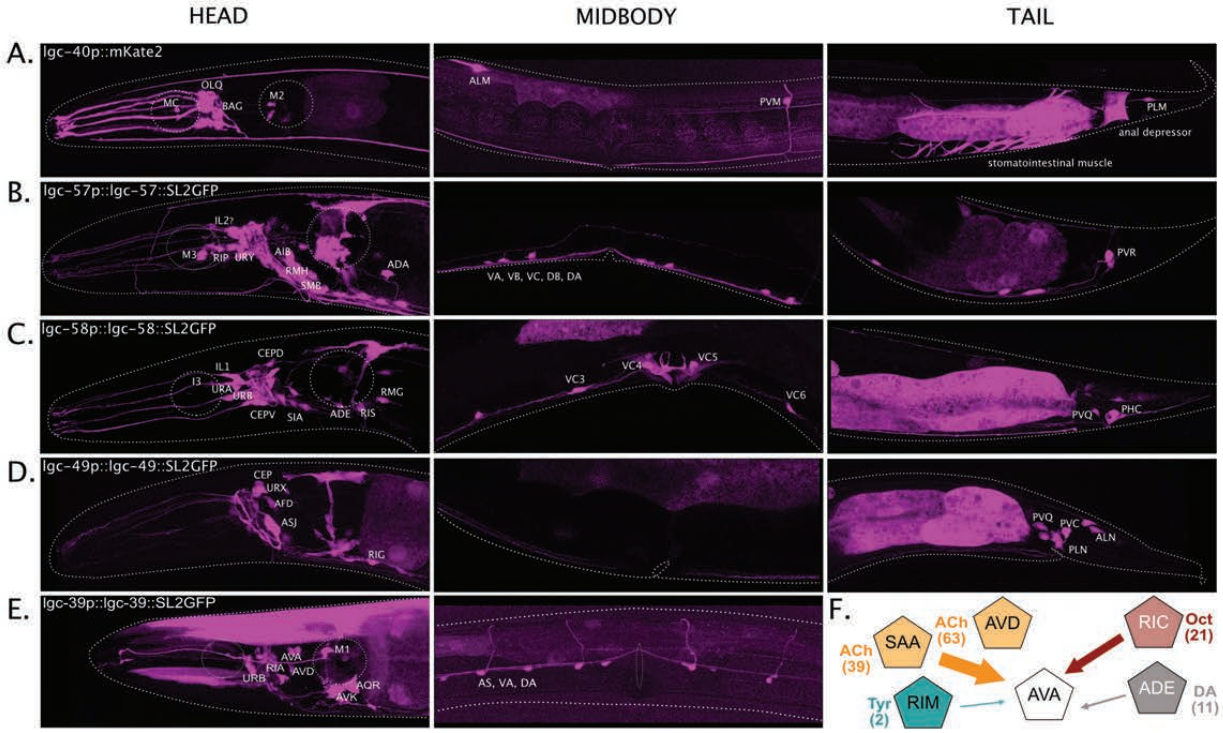

A.

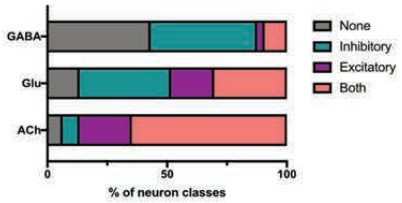

	None	Inhibitory	Excitatory	Both
ACh	6.250	7.031	21.875	64.844
Glu	13.281	38.281	17.969	30.469
GABA	42.969	44.531	3.125	9.375

B.

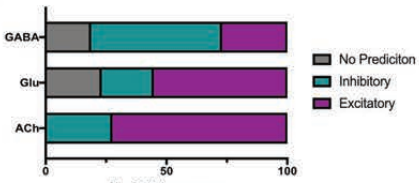

	No Prediciton	Inhibitory	Excitatory
ACh	0.336	27.195	72.469
Glu	23.123	21.542	55.336
GABA	18.710	54.194	27.097

C.

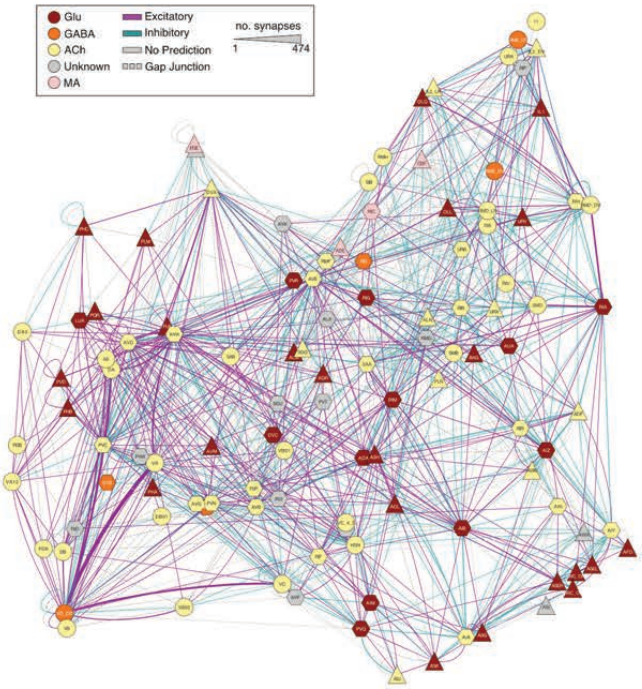

D.